Influence of disorder on electrically and optically detected electron spin nutation

C. Michel,[1,2] A. Gliesche,[1,3] S. D. Baranovskii,[2,*] K. Lips,[4] F. Gebhard,[2] and C. Boehme[1,†]
[1]*Department of Physics, University of Utah, 115S 1400E, Salt Lake City, Utah 84112, USA*
[2]*Department of Physics and Material Sciences Center, Philipps-University, Renthof 5, 35032 Marburg, Germany*
[3]*Institut de Théorie des Phénomènes Physiques, Ecole Polytechnique Fédérale, CH-1015 EPF-Lausanne, Switzerland*
[4]*Helmholtz-Zentrum Berlin für Materialien und Energie (formerly Hahn-Meitner-Institut), Institut fur Silizium-Photovoltaik, Kekuléstrasse 5, D-12489 Berlin, Germany*
(Received 10 January 2009; published 17 February 2009)

A numerical study of the influence of disorder in semiconductors on spin-Rabi nutation observed with pulsed electrically or optically detected magnetic-resonance techniques (pEDMR and pODMR, respectively) is presented. It is shown that transient nutation signals of disordered spin ensembles differ from ordered ensembles as inhomogeneously broadened Landé-factor distributions are presented. In contrast to ordered systems, the magnitudes of spin-Rabi nutation and spin-Rabi beat nutation change significantly with a strong dependence of their ratio on the correlation of the Landé factors within the nearest-neighbor spin pairs. An interpretation of these results is given and their application for the investigation of disorder using pEDMR and pODMR is discussed.

DOI: 10.1103/PhysRevB.79.052201 PACS number(s): 71.23.−k, 61.43.−j, 76.30.−v, 76.70.Hb

There are many ways to classify and quantify the nature of disorder in semiconductors. Structural disorder can be described by radial distribution functions[1] while its influence on electronic properties is reflected by distributions of density of states functions or localization length distributions of electronic states.[2,3] While electron-paramagnetic-resonance (EPR) spectroscopy has also been used for decades to investigate disorder-induced inhomogeneities of paramagnetic electronic states,[4–6] it has been difficult to experimentally determine the correlation lengths of these disorder effects. Correlation lengths are defined by the length scales on which disorder introduces randomization of an observable. For the example of Landé (g) factors, a correlation length represents the distance on which the spin-orbit fields fluctuate affecting the g-factor shifts. EPR resonance lines reflect disorder-induced g factor or coupling strength[6,7] distributions by broadening and deformation of the line shapes. A mathematical deconvolution of EPR lines into distribution functions can therefore bring information about disorder, although this approach is oftentimes not unambiguous.[7] While in recent years, methods for the measurement of dipolar coupling strength distributions using electron-electron double resonance spectroscopy have been demonstrated,[8] experimental approaches to the measurement of correlation lengths of disorder have remained elusive.

In the following we present a numerical study of the influence of disorder on electrically or optically detected spin-Rabi nutation of paramagnetic defects in semiconductors. The aim of this study was to learn how experimental methods such as pulsed electrically and pulsed optically detected magnetic-resonance (pEDMR and pODMR, respectively) spectroscopies can be used to identify influences of disorder on experimental data and how they can reveal insights into the nature of disorder such as estimates for correlation lengths. It is shown that the characteristic dependence of electron spin-Rabi nutation on the excitation frequency can be significantly distorted in disordered host materials. We have investigated these distortions with regard to the interactions between nearest-neighbor spin pairs with the external microwave field and their dependence on the correlation length of disorder. We show that an experimental discrimination of short- (nearest-neighbor) distance versus long-distance disorder using pEDMR or pODMR methods is possible.

pEDMR and pODMR are the combinations of coherent pulsed EPR (pEPR) spectroscopy with electrical or optical detection technique. Spin propagation is observed with these methods via spin-dependent electronic transition rates that influence electric currents or optical transitions.[9] Both pEDMR and pODMR have proven to be extraordinary sensitive methods, in fact they have proven to resolve signals of single spins,[10,11] in contrast to conventional pEPR that is many orders of magnitude less sensitive. The sensitivity advantage of pEDMR and pODMR is of significant importance for spectroscopy of highly diluted or low-dimensional system such as thin film semiconductor materials; many of which exhibit significant disorder. The main difference between pEDMR or pODMR and pEPR lies in the different observables. pEPR as any other pure magnetic-resonance technique is based on the radiative detection of magnetic polarization in coherently propagating spin ensembles. In contrast, pEDMR and pODMR detect spin-dependent rates which means that in many cases electronic transitions whose probability correlates with the singlet content of a pair of two paramagnetic states before a transition occurs. Because of this, many pEDMR and pODMR experiments reveal permutation symmetries of electron spin pairs and not polarization.[9] While this difference of the observable is one of the reasons for the greater sensitivity as it provides high sensitivities even in almost absence of polarization at low magnetic fields,[12] it also has dramatic consequences for the observation of coherent spin motion. A number of recent studies on transient nutation-style experiments of weakly[9,13] and strongly[14] exchange coupled spin pairs showed that pEDMR/pODMR detected nutation frequencies can differ from pEPR detected nutation frequencies, even when both signals are produced by the same spin ensemble. While pEPR is sensitive to the nutation oscillations of electron

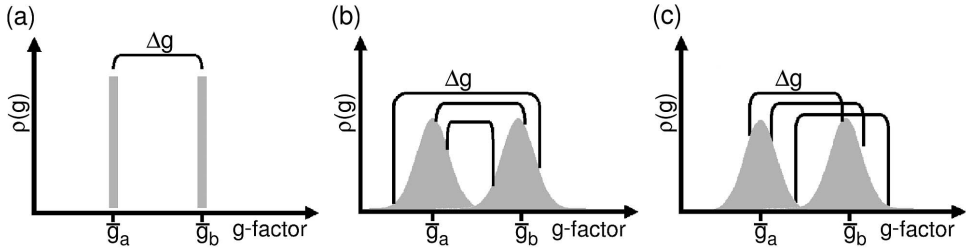

FIG. 1. Sketch of the probability-density distributions of pair constituent g factors g_a and g_b for the different correlation cases considered. (a) g factors are distributed δ-like at their mean values $\bar{g}_a$ and $\bar{g}_b$; Δg is constant for all pairs. (b) and (c) g factors are Gaussian distributed around $\bar{g}_a$ and $\bar{g}_b$, respectively. (b) g factors within the pairs are uncorrelated; Δg varies. (c) g factors within the pairs are correlated; pairs have varying g_a and g_b but $\Delta g=\bar{g}_b-\bar{g}_a=$const. Note: for clarity, $\frac{\delta}{\Delta g}$ is strongly decreased in this sketch in comparison to values used for the calculations.

spins, pEDMR and pODMR are sensitive in addition to nutation beat oscillations. The calculations presented in the following aim to investigate how disorder can change the magnitudes of nutation signals versus the magnitudes of beat signals and how such change depends on the length scales relative to the pair distances on which observed spin-dependent transitions occur in order to show how pEDMR and pODMR measurements can be used to study disorder effects on paramagnetic electron states.

For the calculations, we consider the influence of two types of disorder on electron spin pairs as illustrated in Fig. 1. Disorder causing random g-factor distribution (b) without and (c) with correlation of the g factors within individual spin pairs is shown next to (a) the nondisordered case. Note that disorder-induced g-factor shifts are caused by random local spin-orbit fields due to structural inhomogeneities.[12] Thus, the two disorder cases correspond to random fields that fluctuate (b) on length scales smaller than the spin-pair size and (c) on length scales larger than the spin-pair size. Therefore, different predictions for pEDMR and pODMR experiments for these two cases would allow us to obtain information about the length scales of the spin-orbit field fluctuations and/or spin-pair sizes in disordered materials. The scenarios displayed in Figs. 1(b) and 1(c) are referred in the following as noncorrelated and correlated disorders, respectively.

Our calculations are based on the intermediate-pair model for the description of spin-dependent electron transitions which is described in detail in Refs. 9 and 15. The considered observable is the time integral of length t_0 of a transition-rate transient (e.g., transport or recombination) toward the steady state after a coherent spin excitation of length τ, which for the example of an electrical detection assumes the form of a charge

$$Q(\tau)=\int_0^{t_0} R(t)dt=\sum_{i=1}^{4}\delta\rho_{ii}(\tau)(1-e^{-r_i t_0}), \tag{1}$$

while for radiative transitions $Q(\tau)$ represents a number of photons.[14] The transition-rate coefficients out of a spin-pair eigenstate i are r_i, while $\delta\rho_{ii}(\tau)=\rho_{ii}(\tau)-\rho_{ii}^s(\tau)$ represents the differences of the density-matrix diagonal elements $\rho_{ii}(\tau)$ of the density operator $\hat{\rho}$ and the respective steady-state values ρ_{ii}^s. The density-matrix elements are represented in the base of eigenstates. The dynamics of the spin pairs during an EPR pulse of length τ is described in terms of the stochastic Liouville equation[16]

$$\partial_t\hat{\rho}=\frac{i}{\hbar}[\hat{\rho},\hat{H}]^- +\mathcal{S}[\hat{\rho}]. \tag{2}$$

$\rho_{ii}(t)$ are calculated by solving numerically the set of the corresponding Bloch equations applying a standard Runge-Kutta algorithm. The operator $\mathcal{S}[\hat{\rho}]$ accounting for the stochastic processes such as dissociation, generation, or recombination of pairs can be neglected as it plays no crucial role on the time scales of sufficiently fast coherent spin excitations. The Hamiltonian $\hat{H}$ in Eq. (2) can be decomposed as $\hat{H}=\hat{H}_0+\hat{H}_1$ with $\hat{H}_0=\mu_B B_0[g_a\hat{\sigma}_a^z+g_b\hat{\sigma}_b^z]$ and $\hat{H}_1=\mu_B B_1[g_a\hat{\sigma}_a^x+g_b\hat{\sigma}_b^x]$, where $\hat{H}_0$ describes the Zeeman interaction with a constant magnetic field B_0 oriented in z direction and $\hat{H}_1$ is the Zeeman interaction with the microwave field B_1 which is polarized along the $\hat{x}$ direction in a rotating frame representation.[17] The constant μ_B is the Bohr magneton and $\hat{\sigma}_i^k$ are defined as the Pauli spinors for the two pair partners a and b. Note that in general, an isotropic Heisenberg exchange-coupling contribution $\hat{H}_j=\frac{J}{4}\vec{\sigma}_a\cdot\vec{\sigma}_b$ with exchange-coupling parameter J may need to be necessary for some pair systems.[14] We neglect $\hat{H}_j$ in the following ($J=0$) and discuss the implications of the results for cases where $\hat{H}_j\neq 0$ below. The difference in the strength of the magnetic field to which each of the pair partners is effectively exposed is represented by two different characteristic g factors $\bar{g}_a$ and $\bar{g}_b$ for each of the pair partners.[9,14,15]

In previous studies, disorder in terms of local modifications of the pair partner g factors was completely neglected assuming an ensemble of identical pairs of paramagnetic centers[13,14] with g factors $\bar{g}_a$ and $\bar{g}_b$ as illustrated in Fig. 1(a). In order to take into account the disorder represented by a fluctuation of the g factor on a mesoscopic length scale we consider a Gaussian distribution for both g_a and g_b. The probability of a certain $g_a(g_b)$ is given by

$$p[g_{a(b)}]=\frac{1}{\sqrt{2\pi}\delta}e^{-[g_{a(b)}-\bar{g}_{a(b)}]^2/2\delta^2}. \tag{3}$$

We assume the same standard deviation δ for the distributions of g_a and g_b. We consider an ensemble of $M=81$ non-

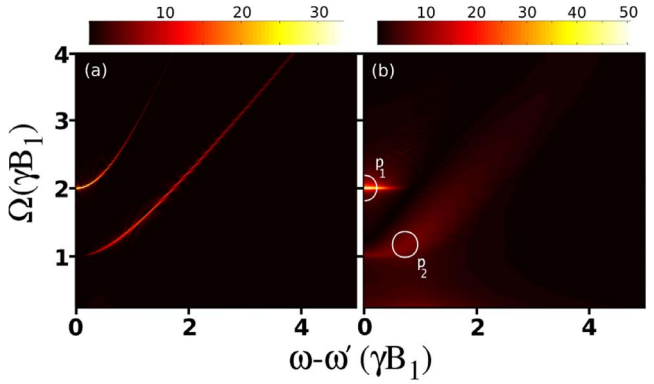

FIG. 2. (Color online) Three-dimensional color plots of the calculated Fourier transform $\Omega(\omega)=\mathrm{FT}[Q(\tau)](\omega)$ of the nutation transient as a function of the excitation frequency ω for the two cases of (a) a homogeneous spin ensemble and (b) a disordered ensemble of 81 pairs provided with random but correlated g factors. All frequencies are scaled in units of γB_1. The frequency scale of ω is offset by the average of the Larmor frequencies of the two pair partners $\omega' = \frac{1}{2}(\omega_a+\omega_b)=10$ GHz while $\frac{\delta}{2\pi}=3$ MHz. The circles indicate the data points with the highest intensities $I(p_1)$ of the $\Omega=2\gamma B_1$ signal and $I(p_2)$ of the $\Omega=\gamma B_1$ signal, respectively.

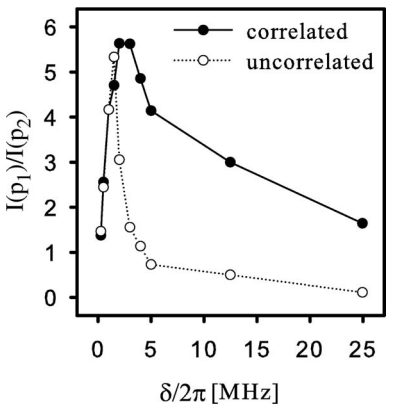

FIG. 3. Plot of the calculated ratio between the intensity of the $\Omega=2\gamma B_1$-nutation beat signal $[I(p_1)]$ and the intensity of the $\Omega=\gamma B_1$-nutation signal $[I(p_2)]$. Note that the frequency range of $0 \leq \delta \leq 25$ MHz was chosen in order to consider cases of $\delta \leq \gamma B_1$ and $\delta \geq \gamma B_1$ since $\gamma B_1 = 10$ MHz.

interacting intermediate pairs whose constituents are numbered by the index i. Each pair is characterized by its two g factors g_a^i and g_b^i. This corresponds to the Larmor frequencies $\omega_a^i = \frac{1}{\hbar} g_a^i \mu_B B_0$ and $\omega_b^i = \frac{1}{\hbar} g_b^i \mu_B B_0$ with $\Delta\omega^i = \omega_b^i - \omega_a^i$.

Figure 2 displays plots of Rabi nutation frequencies as a function of the excitation frequency ω. Two data sets are shown with (a) homogeneous g-factor distributions and (b) inhomogeneous g-factor distributions induced by disorder. In both cases small Larmor separation ($\gamma B_1 \gg \Delta\omega^i$) was assumed for the calculations. Figure 2(a) shows the result of the calculation assuming a deltalike distribution of g factors [Fig. 1(a)]. The two characteristic hyperbola-like signals as discussed in detail in Ref. 13 are clearly visible in the (ω,Ω) plot. Their nutation frequency minima are at $(\omega', 2\gamma B_1)$ due to a nutation beat oscillation of the spin pairs (ω' is the average of the Larmor frequencies of the two pair partners as defined in Fig. 2) and at $(\omega_a, \gamma B_1)$ as well as at $(\omega_b, \gamma B_1)$ due to the individual spin contributions. Due to the small Larmor separation the two different signals at $\omega_a \approx \omega_b$ cannot be distinguished.

When assuming a correlated g-factor distribution $\Delta\omega^i = \text{const}$ with a standard deviation $\frac{\delta}{2\pi}=3$ MHz the results get drastically modified as depicted in Fig. 2(b): (i) The branch of the signal starting at lower Rabi frequency ($\Omega=\gamma B_1$) gets smeared out and is barely visible in contrast to the $\Omega=2\gamma B_1$ signal. (ii) The arms of the $\Omega=2\gamma B_1$ signal almost vanish while for excitation frequencies close to $\omega \approx \omega'$ the signal at $\Omega=2\gamma B_1$ is of dominant intensity.

In order to analyze whether this finding is a general property of a disordered ensemble or whether it is connected to the particular nature of disorder we have performed calculations for ensembles with different standard deviations for both correlated and noncorrelated disorders. In order to quantify the influence of disorder, the ratio of the intensity maxima $I(p_1)/I(p_2)$ of the $\Omega=2\gamma B_1$ and the $\Omega=\gamma B_1$ signals was calculated. Previous studies revealed that without disorder this ratio is ≈ 1.[13,14] In the case of the correlated disorder as shown in Fig. 2(b) this ratio is significantly increased. Note that since the exact position of the signal peaks p_1 and p_2 and their intensity are hardly recognizable on the Fourier plots illustrated in Fig. 2(b), we extracted them directly from the calculated data sets. The result of this procedure is shown in Fig. 3 where the ratio $I(p_1)/I(p_2)$ is plotted against the standard deviation δ of the g-factor distribution for δ being on the order of the induced nutation frequency γB_1. For very small δ the difference between correlated and noncorrelated distributions vanishes as this scenario approaches the deltalike g-factor distribution of ordered ensembles. The p_1 and p_2 signals will assume equal magnitudes in agreement with the data shown in Fig. 2(a). For an increased δ, the results depend on the nature of the g-factor distribution. An ensemble with correlated disorder shows a dominant $\Omega=2\gamma B_1$ signal which has a significantly higher intensity as compared to the maximum of the $\Omega=\gamma B_1$ signal. For the noncorrelated case, an initial increase in $I(p_1)/I(p_2)$ for small values of δ can also be seen. However, this ratio of the two signal intensities drops rapidly even below 1, indicating that the hyperbola-shaped $\Omega=\gamma B_1$ signal becomes dominant.

The numerical calculation of $I(p_1)/I(p_2)$ as a function of δ as displayed in Fig. 3 demonstrates that a noncorrelated disorder of g factors within ensembles of spin pairs leads to a dominance of spin nutation ($\Omega=\gamma B_1$) signals when coherent Rabi nutation is observed through electrical or optical measurement of spin-dependent transport or recombination rates. For the case of disorder with correlated g factors within the spin pairs, spin-beat nutation ($\Omega=2\gamma B_1$) signals will dominate and therefore, the frequency of Rabi nutations observed with the pEDMR or pODMR technique can be an indicator for the correlation lengths of disorder. Our calculations clearly show that disorder causes a disappearance of the characteristic parabola-like signal shapes in Fourier-transformed nutation plots predicted by calculations on homogeneous ensembles without disorder[13,14] when $\delta > \gamma B_1$. We conclude from this observation that the complete absence of these structures in many experimental studies on pODMR

and pEDMR studies of hydrogenated amorphous silicon[7] can be attributed to the effect of disorder.

We want to note that the presented data represent exclusively cases of spin-pair ensembles with small Larmor separation $\Delta\omega^i \ll \gamma B_1$ and negligible isotropic exchange $\hat{H}_J=0$. It shall be emphasized that for large Larmor separated spin ensembles, the g factors within the pairs may or may not be correlated, yet spin nutation beat components will not be visible since there is no influence of beat nutation on spin-dependent transitions when $\Delta\omega^i \gg \gamma B_1$ (Ref. 13) which is the case for large Larmor separation as long as $\delta \ll \Delta\omega^i$. Thus, obtaining boundaries for correlation length using spin nutation frequencies will not be possible in this case. We anticipate the results obtained above to remain, in contrast, fully applicable for cases of strong isotropic exchange within pairs ($J \gg \Delta\omega^i$) in the presence of either large or small Larmor separation. As strong exchange coupling leads to identical nutation patterns with nearly identical signal intensities and parabola-like shapes of the nutation and the beat signals as for the case of small Larmor separation[14] and small exchange considered above, we expect the influence of correlated and noncorrelated disorder to be similar as well. Note, however, that in this case the pEDMR or pODMR signal intensity will be dramatically reduced.[14]

In summary, we have shown by numerical calculations how disorder changes the dominant frequency of electrically or optically detected spin-Rabi nutation of paramagnetic centers involved in spin-dependent electronic transitions. It is shown that disorder determines the intensity ratio of spin-Rabi nutation and spin-Rabi beat nutation signals for the case of correlated g factors of involved spin pairs. Particularly, the dominant resonance at $2\gamma B_1$ in the Rabi-frequency spectrum is found to be a fingerprint of correlated disorder. We predict that a parabola-like shape of Fourier-transformed pEDMR signals known for ordered systems should be converted into a pointlike shape due to effects of disorder. Furthermore the presented calculations provide a tool for detecting the spatial scale of field fluctuations by pEDMR or pODMR experiment.

C.M. is grateful for financial support via the European Graduate College "Electron-electron interactions in solids." Financial support of the Deutsche Forschungsgemeinschaft and that of the Fonds der Chemischen Industrie is gratefully acknowledged.

*baranovs@staff.uni-marburg.de
†boehme@physics.utah.edu

[1] R. J. Temkin, W. Paul, and G. A. N. Connell, Adv. Phys. **22**, 581 (1973).
[2] R. A. Street, *Hydrogenated Amorphous Silicon* (Cambridge University Press, Cambridge, UK, 1991).
[3] *Hydrogenated Amorphous Silicon I and II*, edited by J. Joannopoulos and G. Lucovsky (Springer, New York, 2000).
[4] M. Brodsky and R. Title, Phys. Rev. Lett. **23**, 581 (1969).
[5] H. Dersch, L. Schweitzer, and J. Stuke, Phys. Rev. B **28**, 4678 (1983).
[6] M. Stutzmann and D. K. Biegelsen, Phys. Rev. B **34**, 3093 (1986).
[7] K. Lips, C. Boehme, and T. Ehara, J. Optoelectron. Adv. Mater. **7**, 13 (2004).
[8] G. Jeschke, G. Panek, A. Godt, A. Bender, and H. Paulsen, Appl. Magn. Reson. **26**, 223 (2004).
[9] C. Boehme and K. Lips, in *Charge Transport in Disordered Solids with Applications in Electronics*, edited by S. Baranovski (Wiley, Chichester, England, 2006), Chap. 5, pp. 179–219.
[10] F. Jelezko, T. Gaebel, I. Popa, A. Gruber, and J. Wrachtrup, Phys. Rev. Lett. **92**, 076401 (2004).
[11] M. Xiao, I. Martin, E. Yablonovitch, and H. W. Jiang, Nature (London) **430**, 435 (2004).
[12] J.-M. Spaeth and H. Overhof, *Point Defects in Semiconductors and Insulators* (Springer, Berlin, 2002).
[13] V. Rajevac, C. Boehme, C. Michel, A. Gliesche, K. Lips, S. D. Baranovskii, and P. Thomas, Phys. Rev. B **74**, 245206 (2006).
[14] A. Gliesche, C. Michel, V. Rajevac, K. Lips, S. D. Baranovskii, F. Gebhard, and C. Boehme, Phys. Rev. B **77**, 245206 (2008).
[15] Christoph Böhme, *Dynamics of Spin-Dependent Charge Carrier Recombination* (Cuvillier, Göttingen, 2003).
[16] R. Haberkorn and W. Dietz, Solid State Commun. **35**, 505 (1980).
[17] A. Schweiger and G. Jeschke, *Principles of Pulse Electron Paramagnetic Resonance* (Oxford University Press, Oxford, 2001).